A stochastic model for high Rayleigh number convection

Scott Wunsch * and Alan R. Kerstein
Combustion Research Facility
Sandia National Laboratories, Livermore, CA 94551-0969
(April 28, 2003)
Submitted to *J. Fluid Mech.*

A stochastic one-dimensional model for thermal convection is formulated and applied to high Rayleigh number convection. Comparisons with experimental data for heat transfer in Rayleigh-Beńard cells are used to estimate two model parameters. Reasonable agreement with experimental results is obtained over a wide range of physical parameter values (six orders of magnitude in Rayleigh number, five orders of magnitude in Prandtl number). Using the model, the statistics of fluctuations in the core of the convection cell are studied. Good agreement with available experimental data is obtained. Two distinct pdf shapes are seen; one at low Prandtl number which matches experimental observations, and another at high Prandlt number for which no experimental data exists. The model results are interpreted in terms of two distinct mechanisms for the production of core fluctuations.

I. INTRODUCTION

Turbulent thermal convection has long been recognized as an important aspect of many natural fluid systems, with examples coming from both astrophysics (stars) and geophysics (Earth's atmosphere and molten interior). The physics of thermal convection has typically been studied experimentally using Rayleigh-Beńard systems, in which a cylinder of fluid is heated from below. The resulting density contrast in the fluid generates turbulent motions which transport heat from the lower wall to the top of the cell. The long history of both experimental and theoretical investigations of this system are summarized in Siggia (1994).

The driving force in convective turbulence is the density contrast $\Delta\rho$ induced by the temperature difference between the top and bottom cell walls. In the Boussinesq approximation assumed here, temperature and density variations are proportional and the density difference across the cell is much smaller than the average fluid density ρ_o. The strength of the driving force is expressed in dimensionless form by the Rayleigh number Ra, defined as

$$Ra \equiv \frac{g\Delta\rho\Lambda^3}{\rho_o\nu\kappa} \tag{1}$$

where g is the gravitational acceleration, Λ is the distance separating the walls, ν is the kinematic viscosity, and κ is the molecular diffusivity. Two other parameters also govern the behavior of the system. One is the Prandtl number, $Pr \equiv \nu/\kappa$, which measures the relative strengths of the molecular processes. It is determined by the choice of working fluid. The other is the aspect ratio of the cell; the ratio of cell diameter (assuming a cylindrical cell) to cell height. Natural systems might be considered to correspond to infinite aspect ratio cells, although in many natural systems the upper or lower boundaries may also differ from hard walls. The most often measured quantity in convective cells is the heat transfer rate, which is expressed in dimensionless terms by the Nusselt number Nu, defined as the ratio of the turbulent heat transfer at the walls to the hypothetical heat transfer in quiescent fluid due to molecular conduction. The classical assumption that the heat transfer should be independent of the height Λ for large Ra yields the scaling

$$Nu \sim Ra^{1/3} \tag{2}$$

based on dimensional analysis (Siggia 1994). Experimental results in Rayleigh-Beńard cells generally indicate scaling laws with exponents less than 1/3, with the actual value depending on Pr. A recently proposed scaling analysis by Grossmann & Lohse (2000, 2001, 2002) attempts to explain these non-classical scaling laws by considering the dissipation of energy and thermal fluctuations in the cell.

Although much attention has been paid to understanding the non-classical behavior of the heat transfer, the turbulent fluctuations of the density (or temperature) in the core of the Rayleigh-Beńard cell are also of interest and are the primary focus of this study. The typical magnitude of the density fluctuations has been observed to scale with Ra (Castaing *et al.* 1989; Niemela *et al.* 2000). The magnitude also shows a dependence on cell geometry, although the

*email: sewunsc@sandia.gov

probability distribution function (pdf) of the fluctuations does not (Daya & Ecke 2001). Understanding how the shape of the pdf depends on physical flow parameters and boundaries is important for generalizing experimental observations to natural convecting systems in geophysics and astrophysics. Knowing the likelihood of large temperature fluctuations is especially important in reacting flows, since reaction rates have a strongly nonlinear temperature dependence.

In this work a stochastic one-dimensional model is used to study high Rayleigh number convection. The model is a version of the 'One-Dimensional Turbulence' (ODT) model created by Kerstein (1999) and has been previously applied to stably stratified turbulence (Wunsch & Kerstein 2001, Wunsch 2003). Comparisons with heat transfer measurements in Rayleigh-Beńard cells are performed to set parameters and validate the performance of the model. Since the one-dimensional model cannot reproduce the important effects of cell geometry and side-wall heat loss, perfect agreement with experiment is not expected. Instead, the goal is to reproduce the approximate Nu at a given Ra and Pr so that the correct flow conditions are obtained to permit study of the interior fluctuations. Unlike simple scaling theories, the stochastic, time-dependent nature of this model allows a detailed study of the statistics of fluctuations in the core of the cell. This data is compared with experimentally measured statistics (where available) and provides insight into the convection processes that govern the likelihood of fluctuations.

The advantages and disadvantages of this modelling approach relative to other forms of numerical simulation are worth mentioning. First and foremost, the restriction to one dimension makes the model much more computationally affordable than direct numerical simulation. This makes it possible to explore the parameter space of Ra and Pr much more efficiently. Published studies of the Prandtl number dependence of the heat transfer rate using direct numerical simulation have been performed only at the modest Rayleigh numbers of $Ra = 10^6$ (Verzicco & Camussi 1999) and $Ra = 10^7$ (Kerr & Herring 2000), while exploration of the dependence on Ra at near-unity Prandtl number have reached $Ra = 2 \cdot 10^9$ (Verzicco 2002). This last study required a total of $1.6 \cdot 10^6$ mesh nodes, while our model simulations of the same case require only $1.6 \cdot 10^4$ mesh nodes. The ODT simulations are also carried out for much longer times to collect accurate statistical information on temperature fluctuations (10^3 to 10^5 large eddy turnover times, compared to 20 to 50 turnover times for typical direct numerical simulations). Of course, the advantage of full three-dimensional numerical simulation is that all relevant effects, including geometry and side-wall heat transfer, are captured, which is not the case in the model. However, these effects are negligible in many natural systems, and the ODT model therefore might be well-suited to future studies of those flows.

A more efficient approach to simulating the effects of geometry on a convecting flow is the use of large eddy simulation (Kimmel & Domaradzki 2000), or LES, which neglects the smaller scales. However, this technique does not allow the study of small-scale fluctuations. The model used in this work is therefore complementary to large eddy simulation, in the sense that LES incorporates geometry but parameterizes the effects of small-scale fluctuations, while the opposite is true of ODT.

II. ONE-DIMENSIONAL MODEL

A. Overview

The density structure of a convecting system is a function primarily of the vertical coordinate y. Hence it is plausible that a one-dimensional model might describe the physics of the problem. The approach used here is a version of the ODT model created by Kerstein (1999); the specific version is identical to the one applied to stably stratified turbulence in Wunsch & Kerstein (2001) and Wunsch (2003), except for the boundary conditions and forcings. Only a brief summary of the model will be presented here; the reader is referred to the earlier literature for additional details.

Two scalar fields, each a function of vertical position y and time t, are used to describe convecting systems in this model. One is a density scalar, defined as $\delta\rho(y,t) \equiv \rho(y,t) - \rho_o$, which represents a vertical profile of density fluctuations in the convective cell. The reference density ρ_o is taken to be the fluid density at the lower plate, so that $\delta\rho \geq 0$. The other is a 'velocity' scalar, $v(y,t)$, whose square represents a vertical profile of kinetic energy in the cell. It is not a real velocity in the sense that it does not directly advect itself or the density scalar. Rather, it is used simply as a kinetic-energy surrogate in the model.

In ODT, advection consists of randomly chosen measure-preserving mapping events that rearrange the scalar fields. Each mapping is a local event, with a well-defined position y_o and spatial extent l, and each event is loosely interpreted as corresponding to a turbulent 'eddy' of size l in the flow. Mappings are possible on all scales and represent all scales of convective motions. (For example, mappings on the largest scale Λ represent the large-scale convective roll observed in Rayleigh-Beńard cells.) The mapping function is designed to 'wrinkle' the flow, reducing length scales within the affected interval. In addition, the mappings induce net scalar transport in the presence of a gradient. The times and

locations of the mapping events are selected at random from a rate distribution whose functional dependence on the local ODT variables $\delta\rho(y,t)$ and $v(y,t)$ is based on the energetics of turbulence.

Using simple energetic scaling arguments, a characteristic frequency can be inferred for each possible eddy in the system, thereby determining an event rate distribution corresponding to the current state of the system. The model then randomly samples all possible eddies with the assigned frequencies. During the time intervals between these instantaneous mappings, the scalar fields evolve according to the molecular transport equations:

$$\left(\partial_t - \nu\partial_y^2\right) v(y,t) = 0 \tag{3}$$

$$\left(\partial_t - \kappa\partial_y^2\right) \delta\rho(y,t) = 0. \tag{4}$$

Boundary conditions are applied at the top ($y = \Lambda$) and bottom ($y = 0$) of the box, so that $v(y=0) = v(y=\Lambda) = 0$, $\delta\rho(y=0) = 0$ and $\delta\rho(y=\Lambda) = \Delta\rho$. These equations are solved as a time-sequence of initial value problems, each starting immediately after a mapping event and proceeding until the time of the next mapping event.

The ODT model contains four basic elements necessary for exploring turbulent convecting flows: energy conservation, scalar transport, multiscale dynamics, and molecular dissipation. The restriction to one computational dimension makes it possible to efficiently study a wider range of parameter space than is possible by direct numerical simulation.

B. Eddy Definition

The fundamental dynamical object in the model is the advective mapping. It consists of a measure-preserving map $f(y)$ of the domain onto itself, so that any scalar field undergoes the transformation $v(y) \to v(f(y))$ when acted on by the map. The mapping acts on a segment of length l, from position y_o to y_o+l. It is loosely interpreted as representing the effects of an 'eddy' of size l on the scalar fields. The velocity and density scalars are both mapped to mimic the transport of fluid elements. The particular mapping function is arbitrary, but we choose a piecewise-linear function as a convenient way to meet the requirements of measure preservation and finite extent. As in previous ODT work, we use a three-piece function which takes the line segment, shrinks it to a third of its original length, and then places three copies on the original domain. The middle copy is reversed, so that the mapped field $v(f(y))$ is continuous if $v(y)$ is continuous. The mapping function reduces to the identity map $f(y) = y$ outside of the mapped interval.

The rearrangement of the density field by the mapping alters the total potential energy, but the mapping itself leaves the total kinetic energy unchanged. To enforce energy conservation, a function $K(y)$ of specified form is added to the velocity field whenever an eddy occurs. The mapping induces displacements of $y - f(y)$. This is a natural candidate for the energy exchange function, so we assume $K(y) = y - f(y)$. This function is non-zero only within the mapped region.

Thus, under the action of an eddy, the density and velocity fields undergo the transformations

$$\begin{aligned} \delta\rho(y) &\to \delta\rho(f(y)) \\ v(y) &\to v(f(y)) + cK(y). \end{aligned} \tag{5}$$

The amplitude c of the energy exchange term $cK(y)$ is determined for each eddy individually to achieve energy conservation.

To calculate c, the energetic consequences of applying (5) must be assessed. The energy E is defined as

$$E \equiv \frac{1}{2}\rho_o \int v^2(y)\mathrm{d}y + g\int \delta\rho(y) y \mathrm{d}y \tag{6}$$

To achieve energy conservation, the amplitude c in (5) must be determined so that the energy is unchanged by the action of the eddy. This yields

$$c = \frac{27}{4l}\left(-v_K \pm \sqrt{v_K^2 - \frac{8}{27}\frac{\rho_K}{\rho_o} gl}\right) \tag{7}$$

where

$$s_K \equiv \frac{4}{9l^2}\int_{y_o}^{y_o+l} s(y)\left[l - 2(y-y_o)\right]\mathrm{d}y \tag{8}$$

and s denotes either v or $\delta\rho$. This solution is not necessarily real; eddies that do not yield a real value for c are assumed to be energetically prohibited (more details later). The solution branch is chosen so that $c = 0$ if $\rho_K = 0$. This implies using the '+' sign in (7) whenever $v_K > 0$, and the '-' sign otherwise. There is an ambiguity if $v_K = 0$ that is resolved using a random perturbation procedure. Using the value of c given by (7) for each mapping event, $cK(y)$ is added to v after the mapping.

C. Eddy Selection

The final ingredient required in the model is to determine the time sequence of eddies, each parameterized by position y_o and size l. To estimate a time scale for each possible eddy, consider the Sharp-Wheeler turnover time $\tau(y_o, l; t)$ for eddies driven by an unstable density difference $\hat{\rho}$: $\tau \sim \sqrt{l\rho_o/(g\hat{\rho})}$. In real turbulence, this is roughly the time required for a region of size l to convectively mix. In ODT, eddies are implemented instantaneously, but eddies in a given order-one range of size and location should occur approximately once each turnover time. In ODT, τ is determined by analogy with the Sharp-Wheeler time, but expressed in terms of energy by assuming that $(l/\tau)^2$ is proportional to the potential energy change $(-8gl\rho_K/27\rho_o)$ due to the mapping:

$$\left(\frac{l}{\tau}\right)^2 \sim -\frac{8}{27}\frac{\rho_K}{\rho_o}gl. \tag{9}$$

While density fluctuations are the primary drivers of eddy turnovers in the flows considered here, kinetic energy also contributes. The typical turnover time for eddies in the absence of density differences scales as $\tau(l) \sim l/\tilde{v}(l)$, where $\tilde{v}(l)$ is some measure of the velocity fluctuations. A convenient velocity measure for determining the turnover time for individual eddies is v_K, defined by (8). Both density and velocity contributions need to be included in determining the eddy turnover times. While the precise functional form is arbitrary, we choose a linear combination of the form

$$\left(\frac{l}{\tau}\right)^2 \sim v_K^2 - \frac{8}{27}\frac{\rho_K}{\rho_o}gl - Z\frac{\nu^2}{l^2} \tag{10}$$

for consistency with the ODT energy conservation mechanism (7). Eddies whose τ values are imaginary are of course prohibited by energetic considerations. The third term on the right hand side of eq. 10 is included to prohibit eddies smaller than the viscous damping scale from occuring. It is negligible at larger scales. The constant of proportionality Z in the viscous damping term is a parameter of the model.

The time scales τ for all possible eddies are translated into an eddy rate distribution λ, defined as $\lambda(y_o, l; t) \equiv C/l^2\tau(y_o, l; t)$. All of the interesting physics is subsumed in τ (10), while the dimensionless constant C is a parameter of the model. Using the turnover time in (10), the eddy rate distribution is given by

$$\lambda = \frac{C\nu}{l^4}\sqrt{\left(\frac{v_K l}{\nu}\right)^2 - \frac{8g}{27\nu^2}\frac{\rho_K}{\rho_o}l^3 - Z}. \tag{11}$$

The actual rate of an eddy with position between y_o and $y_o + dy_o$ and length in the range between l and $l + dl$ is given by $\lambda(y_o, l)dy_o dl$. One can see that, in the absence of gravity, a 'local Reynolds number,' $v_K l/\nu$, determines the rate of each eddy. Buoyant forces either enhance or lower the effective local Reynolds number. The construction of the ODT eddy rate given above utilizes two free parameters, C and Z. The overall rate parameter C determines the strength of the turbulence in the model.

The model is basically an application of mixing length theory locally throughout the model domain, defining a wide range of possible mixing lengths l and corresponding time scales τ that depend on the current local flow structure as well as on l. Turbulent mixing is randomly applied throughout the system on all length scales based on the locally appropriate time scales.

Given initially motionless fluid and an initially constant density gradient $\Delta\rho/\Lambda$ in the cell, the measure of the density fluctuations that drive an eddy of size l is $\rho_K = -\frac{2\Delta\rho l}{27\Lambda}$. Hence an eddy of size l yields a real value of λ based on (11) only if $Ra \geq \left(\frac{27}{4}\right)^2 ZPr\left(\frac{\Lambda}{l}\right)^4$. Since the ODT model is based on turbulence scalings, it only makes sense when applied to problems in which the Rayleigh number is sufficiently large to permit a range of eddy sizes to occur. A rough estimate of this condition is obtained by requiring λ to be real for eddies of size $l \sim 0.1\Lambda$ in the initial configuration. This yields

$$Ra \geq 10^5 ZPr \tag{12}$$

as the approximate condition for well-developed turbulence in the model. This sets a lower limit on the allowable value of Ra for any given Pr in the model.

D. Conservation Laws

Because the eddies do not alter the energy in the system, boundaries and viscous dissipation are the only sources of energy change. Using the differential equations for the dissipative processes, it is straightforward to form an equation for the energy change:

$$\partial_t E = g\kappa \int y\partial_y^2 \delta\rho \mathrm{d}y + \nu\rho_o \int v\partial_y^2 v \mathrm{d}y = g\kappa\Delta\rho \left(\frac{\Lambda}{\Delta\rho} \partial_y \delta\rho|_{y=\Lambda} - 1 \right) - \nu\rho_o \int (\partial_y v)^2 \mathrm{d}y \tag{13}$$

The rate of energy change jumps instantaneously when an eddy occurs, but the total energy itself is not changed by the eddy. In a statistical steady state the energy change is, on average, zero ($\langle \partial_t E \rangle = 0$), and this case implies the relation

$$Ra(Nu - 1) = Pr^2 \epsilon \tag{14}$$

where the Nusselt number Nu is defined as

$$Nu \equiv \frac{\Lambda}{\Delta\rho} \langle \partial_y \delta\rho(y) \rangle|_{y=\Lambda} \tag{15}$$

and the dimensionless energy dissipation ϵ is

$$\epsilon \equiv \frac{\Lambda^3}{\nu^2} \int \langle (\partial_y v)^2 \rangle \mathrm{d}y. \tag{16}$$

There is an additional conservation law for the density variance, $\delta\rho^2$. Since eddies preserve all moments of the density field, only the boundaries and molecular dissipation alter the variance. Again, it is straightforward to form the conservation law

$$\partial_t \int \delta\rho^2 \mathrm{d}y = 2\kappa \int \delta\rho \left(\partial_y^2 \delta\rho \right) \mathrm{d}y = 2\kappa \left(\delta\rho \partial_y \delta\rho \right) |_0^\Lambda - 2\kappa \int \left(\partial_y \delta\rho \right)^2 \mathrm{d}y. \tag{17}$$

In statistical steady state this implies

$$\epsilon_\rho \equiv \frac{\Lambda}{\Delta\rho^2} \int_o^\Lambda \langle (\partial_y \delta\rho)^2 \rangle \mathrm{d}y = Nu. \tag{18}$$

The conservation relations (14) and (18) are the one-dimensional analogs of the general conservation laws for three-dimensional convection (Siggia 1994).

III. NUMERICAL IMPLEMENTATION

To render the ODT model in non-dimensionalized form for numerical simulation, it is necessary to rescale the length, time, velocity, and density variables by reference values. The obvious length scale for rescaling is the cell height Λ. The dimensionless position y' and eddy size l' are defined by $y' \equiv y/\Lambda$ and $l' \equiv l/\Lambda$. Time is rescaled in terms of the time scale for viscous smoothing of cell-scale structures: $t' \equiv t\nu/\Lambda^2$.

The velocity is rescaled in terms of y'/t': $v' \equiv Cv\Lambda/\nu$. Due to the inclusion of C in the dimensionless velocity, physical velocities are rescaled from model velocities by the model constant C. The time evolution equation for the velocity field becomes

$$\frac{\partial v'}{\partial t'} = \frac{\partial^2 v'}{\partial y'^2}. \tag{19}$$

The density field $\delta\rho$ is non-dimensionalized by the density difference $\Delta\rho$ across the cell: $\delta\rho' \equiv \delta\rho/\Delta\rho$. The time evolution equation for the density field is

$$\frac{\partial \delta\rho'}{\partial t'} = \frac{1}{Pr} \frac{\partial^2 \delta\rho'}{\partial y'^2} \tag{20}$$

where $Pr \equiv \nu/\kappa$ is the Prandtl number. Since density is linearly related to temperature in most convection experiments, the normalized density field is equivalent to a normalized temperature field.

The rescaled eddy rate is

$$\lambda' = \frac{1}{l'^4} \sqrt{\left(l' v'_K \right)^2 - g' \rho'_K l'^3 - ZC^2}, \tag{21}$$

where the dimensionless gravity is $g' \equiv \frac{8C^2\Delta\rho\Lambda^3}{27\rho_o\nu^2}g$. The dimensionless measure of velocity and density fluctuations is

$$s'_K \equiv \frac{4}{9l'^2}\int_{y'_o}^{y'_o+l'} dy' s'(y')(l' - 2(y' - y'_o)). \tag{22}$$

where s denotes v or ρ, and the dimensionless energy-exchange amplitude (7) is

$$c' = \frac{27}{4l'}\left(-v'_K \pm \sqrt{v'^2_K - g'\rho'_K l'}\right). \tag{23}$$

The ODT model now contains a single meaningful model parameter ZC^2, as well as the physical control parameters g' and Pr. The physical Rayleigh number (1) can now be expressed as

$$Ra = \frac{27}{8C^2}Prg' \tag{24}$$

where C is the ODT rate parameter, which allows the freedom to rescale the physical Rayleigh number.

The ODT model consists of the continuous implementation of molecular processes based on (19) and (20) for the velocity and density fields, punctuated by discrete advection events (eddies). Eddies are randomly selected with rates given by (21) and (22). Details of the sampling process can be found in Kerstein (1999). All eddy sizes (from the grid resolution to the entire cell height) and locations are sampled, but (21) determines which are implemented in a grid-independent manner. When an eddy is implemented, both fields are advected by the triplet map, and then $c'K(y)$ is added to the velocity field (to conserve energy), where the amplitude c' is given by (23).

In numerical implementation, a first-order implicit finite difference scheme was applied for solution of the molecular process equations. The continual rearrangement of the fields by eddies eliminates any need for sophisticated numerical techniques, since more accurate information is naturally destroyed by the random motions. Grid resolution was sufficient so that the smallest eddy size was 24 to 1000 times the grid point separation, depending on the Prandtl number. Up to 65,536 grid points were used. Simulations were run until a statistically steady state was achieved before any data collection was undertaken.

IV. SIMULATION RESULTS

Figure 1 shows the density profile resulting from a typical simulation. The profile indicates two thermal boundary regions near $y \sim 0$ and $y \sim \Lambda$, seperated by a core mixed region. The instantaneous profile shows a number of significant fluctuations; in the averaged profile these are smoothed away. The Nusselt number is calculated using the slopes of the averaged profile at the walls. Statistics of the density and velocity fluctuations are sampled in the well-mixed core region.

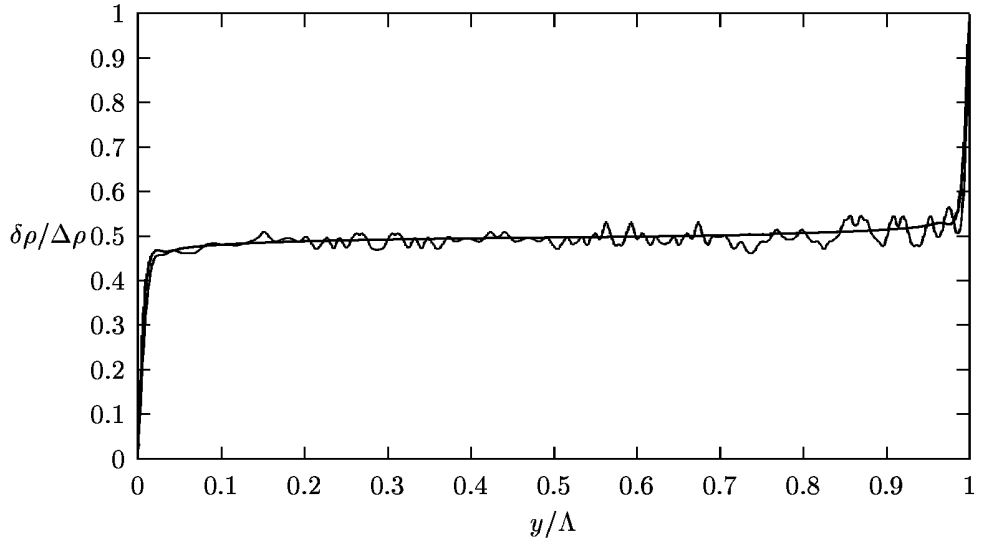

FIG. 1. Typical ODT instantaneous (bumpy line) and average (smooth line) density profiles. Taken from a simulation with $RaC^2 = 10^{12}$, $Pr = 4$, and $ZC^2 = 10^5$.

The ODT model has no explicit mechanism for representing side walls, and conceptually seems most comparable to the infinite-aspect-ratio limit. Vertical motions of all sizes in ODT have the same dynamical form (the eddy mapping). However, in low-aspect-ratio (tall and thin) cells, large vertical motions are influenced by the presence of the side walls, while smaller motions in the interior of the cell are not. On the other hand, in large-aspect-ratio cells and in many geophysical and astrophysical convection problems, vertical motions as large as the cell height can occur in the cell interior with minimal influence from the side walls. In this case all dynamical length scales are free from side-wall distortion, which is analogous to ODT. Hence the model has no way to represent the geometry dependence that has recently been reported for low-aspect-ratio convection cells (Daya & Ecke 2001). In addition, the model lacks any representation of the effects of imperfectly insulating side-walls, whose effects may play a significant role in Rayleigh-Beńard cells (Roche, *et. al.* 2001, Verzicco 2002). Variations in the way in which this effect is accounted for by different groups unfortunately complicates the interpretation of experimental heat transfer measurements (Ahlers & Xu 2001). However, in the absence of data from true infinite-aspect-ratio flows, heat transfer measurements from finite cells are used to estimate plausible values of the model parameters C and ZC^2. The goal is not to explain the observed values of Nu, but rather to ensure that reasonable heat transfer rates are produced by the simulations to facilitate proper study of the core fluctuations.

A. Heat Transfer, $Nu(Ra, Pr)$

To illustrate the role of the model parameters ZC^2 and C, simulations with a range of Prandtl numbers were performed at a Rayleigh number of $Ra = 10^9$ for three different values of ZC^2: 823, 10^4, and 10^5. The results are shown in figure 2, along with a number of experimental results. The value of C, which essentially shifts the curves vertically (by changing the physical Ra which corresponds to a given model parameter RaC^2) was chosen so that the ODT data would approximately match the experimental point shown at $Pr = 0.025$ (liquid mercury convection). Actual values were $C^2 = 800$ for $ZC^2 = 823$, $C^2 = 1200$ for $ZC^2 = 10^4$, and $C^2 = 1500$ for $ZC^2 = 10^5$. The value of C needed changes only modestly because, at low Pr, the heat transfer rate becomes independent of viscosity and hence independent of the viscous cut-off parameter Z. One can see that the curve $Nu(Pr)$ peaks at a value of Pr which depends on the ODT parameter ZC^2, and that for larger Prandtl numbers the heat transfer varies strongly with Z, since viscosity is a significant factor in the limit $Pr \to \infty$. The peak value occurs at approximately $Pr \sim 20$ for $ZC^2 = 823$, $Pr \sim 5$ for $ZC^2 = 10^4$, and $Pr \sim 2$ for $ZC^2 = 10^5$. The precise location of the peak of $Nu(Pr)$ is not clear from the experimental data; however, numerical simulations by Kerr & Herring (2000) suggest that it occurs near $Pr = 2$ for $Ra = 10^7$. At large Pr, the trend of Nu decreasing as Pr increases seen in the experiments of Ahlers & Xu (2001) and Xia, Lam & Zhou (2002) also appears in the ODT data, although the rate of decrease is slightly larger in the model.

A number of experimental results are shown in figure 2 for comparison to the ODT data. In all cases, values of Nu were estimated from published scaling laws which approximate the original data, which was not available in the literature. All of the data shown were taken in cylindrical convection cells with an aspect ratios of either 0.5 or 1.0. Changes in the aspect ratio modestly influence the value of Nu, as discussed in Wu & Libchaber (1992). A brief discussion of the source of each of these results is included below.

Liquid mercury is the working fluid with the lowest Prandtl number ($Pr = 0.025$) yet attained in a convection cell. Cioni, Ciliberto & Sommeria (1997) report an approximate scaling law $Nu = 0.14Ra^{0.26}$ in a unit aspect ratio cell over the range $5 \cdot 10^6 \leq Ra \leq 5 \cdot 10^9$. This experiment suggests $Nu \simeq 30$ at $Ra = 10^9$. Takeshita *et. al.* (1996) report a scaling of $Nu = 0.155Ra^{0.27}$ in the range $10^6 \leq Ra \leq 10^8$, which extrapolates to a significantly higher value of $Nu \simeq 40$ at $Ra = 10^9$. Hence figure 2 presents the average ($Nu = 35$) of these two experiments. The earlier results of Rossby (1969) are neglected because the maximum Ra achieved in that work was only $5 \cdot 10^5$.

In recent years there have been many experimental studies of helium convection ($Pr \simeq 0.7$) in cells with various aspect ratios. The work of Niemela *et al.* (2000) indicate an approximate scaling of $Nu = 0.124Ra^{0.309}$ over the enormous scaling range $10^6 \leq Ra \leq 10^{17}$, yielding an approximate value of $Nu \simeq 75$ at $Ra = 10^9$. This is a different scaling exponent from the previous work of Castaing *et al.* (1989), which reports $Nu = 0.17Ra^{0.29}$ for Ra up to 10^{14}, also for an aspect ratio 0.5 cell. However, the actual Nu value at $Ra = 10^9$ is $Nu \simeq 69$ in the earlier work, which is only an 8% discrepancy. It is asserted in Niemela *et. al.* (2000) that this difference is due to inaccuracies in the properties of helium used to analyze the earlier results. Other results for helium convection report approximate values of Nu at $Ra = 10^9$ of $Nu \simeq 80$ (Wu & Libchaber 1992), $Nu \simeq 75$ (Chavanne *et al.* 1997), and $Nu \simeq 70$ (Chavanne *et al.* 2000). Figure 2 therefore shows $Nu = 75$ for helium convection, representing a number of experiments which indicate that Nu lies in the range $70 - 80$ at $Ra = 10^9$.

Several older experiments have studied convection in water ($Pr \simeq 6$) cells (Garon & Goldstein 1973; Goldstein & Tokuda 1980; Tanaka & Miyata 1980). They cover relatively limited ranges of Ra (typically only two orders of

magnitude), including $Ra = 10^9$. Reported scaling results for large aspect ratio experiments are $Nu = 0.13Ra^{0.293}$ (Garon & Goldstein 1973) and $Nu = 0.145Ra^{0.29}$ (Tanaka & Miyata 1980), which yield estimates $Nu \simeq 56$ and $Nu \simeq 59$ at $Ra = 10^9$, respectively.

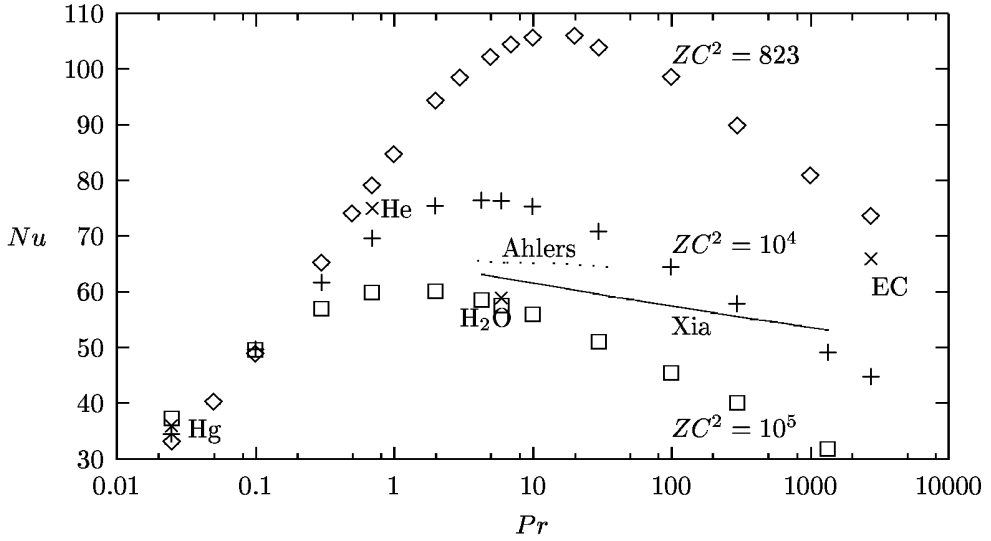

FIG. 2. Nu as a function of Pr from ODT simulations with $Ra = 10^9$. Three values of the model constant ZC^2 are shown: $ZC^2 = 823$ (diamonds), $ZC^2 = 10^4$ (crosses), and $ZC^2 = 10^5$ (squares). For comparison, experimental data ($\times$) are shown for mercury (Hg), helium (He), water (H_2O), and electrochemical convection (EC). Also shown are experimental data (lines) using different fluids to cover a range of Pr in the same apparatus (Ahlers & Xu 2001, Xia, Lam & Zhou 2002).

Ahlers & Xu (2001) recently studied convection using four organic fluids with Prandtl numbers in the range $4 \leq Pr \leq 34$ for Rayleigh numbers up to 10^{11} using aspect ratio 0.5 and 1.0 cells. They do not report a scaling law for their data, but by reading from their figures it can be estimated that the Nusselt number decreases from $Nu \simeq 65.5$ at $Pr \simeq 4$ to $Nu \simeq 64.5$ at $Pr \simeq 34$ for the aspect ratio 0.5 cell. Results are a few percent lower for the unit-aspect-ratio cell. These results utilize a model to correct the measured heat current at the walls, and they note that if this model was applied to the helium convection data of Niemela *et al.* (2000), the result would be to lower the Nusselt number from $Nu \simeq 75$ to $Nu \simeq 60$ at $Ra = 10^9$. However, in figure 2 we choose to present the helium data as published by the original authors, without corrections suggested by subsequent authors.

Another experiment using a variety of liquids to study convection over a range of Prandtl number in the same unit-aspect-ratio cell has been conducted by Xia, Lam & Zhou (2002). They use nine working fluids covering the range $4.3 \leq Pr \leq 1352$. The Rayleigh number range is $2 \cdot 10^7 \leq Ra \leq 3 \cdot 10^{10}$, although no single fluid spans this entire range. They do not report results for individual fluids, but instead summarize their data with the approximate relationship $Nu = 0.14Pr^{-0.03}Ra^{0.297}$. This scaling is used to produce the $Nu(Pr)$ curve shown in figure 2. At $Pr = 4$ their results are very similar to the (corrected) results of Ahlers & Xu (2001), but the decrease of Nu as Pr increases is more pronounced in their work.

The scaling of Nu with Ra at $Pr \simeq 2750$ has been explored using electrochemical convection by Goldstein, Chiang & See (1990). They report $Nu \simeq 0.0659Ra^{1/3}$ over the range $3 \cdot 10^9 \leq Ra \leq 5 \cdot 10^{12}$ in a large-aspect-ratio cell. Extrapolating this scaling to $Ra = 10^9$ gives $Nu \simeq 66$, which is 25% larger than an extrapolation of the results of Xia *et al.* (2002) would give for the same Ra and Pr.

Comparing ODT and experimental data in figure 2, one sees that there is good agreement with the mercury data, since the ODT parameter C was chosen to achieve this. The ODT results for $ZC^2 = 823$ and $ZC^2 = 10^4$ both fall near the range of observed Nu values for helium. The $ZC^2 = 10^5$ data underpredict Nu for He but match the water data well. The $ZC^2 = 10^4$ and $ZC^2 = 10^5$ data bracket the results of Ahlers & Xu (2001) and Xia *et al.* (2002). Simulation and experiment both exhibit a trend of decreasing Nu as Pr increases, but the trend is slightly stronger in the ODT data than in the experiments. The $ZC^2 = 823$ data best match the electrochemical convection result (the value $ZC^2 = 823$ was selected to match that experiment), which indicates a much larger value of Nu than would be expected based on the results of Xia *et al.* (2002). No attempt to resolve this discrepancy is made here.

Figures 3 and 4 illustrate the dependence of Nu on Ra in the ODT model for $ZC^2 = 10^4$ and 10^5, respectively, and several different values of Pr. Experimental results shown for comparison were selected to be representative of a wide range of Pr values; all possible experiments cannot be shown without loss of clarity. The vertical axis shows

$NuRa^{-1/3}$, so that horizontal lines would indicate purely classical scaling. All ODT data exhibit approximate scaling exponents in the range 0.27 to 0.33, depending on Pr and Ra. Plotting $NuRa^{-1/3}$ also magnifies differences between ODT and experimental results, since actual values of Nu vary by more than two orders of magnitude while values of $NuRa^{-1/3}$ vary only by a factor of about two.

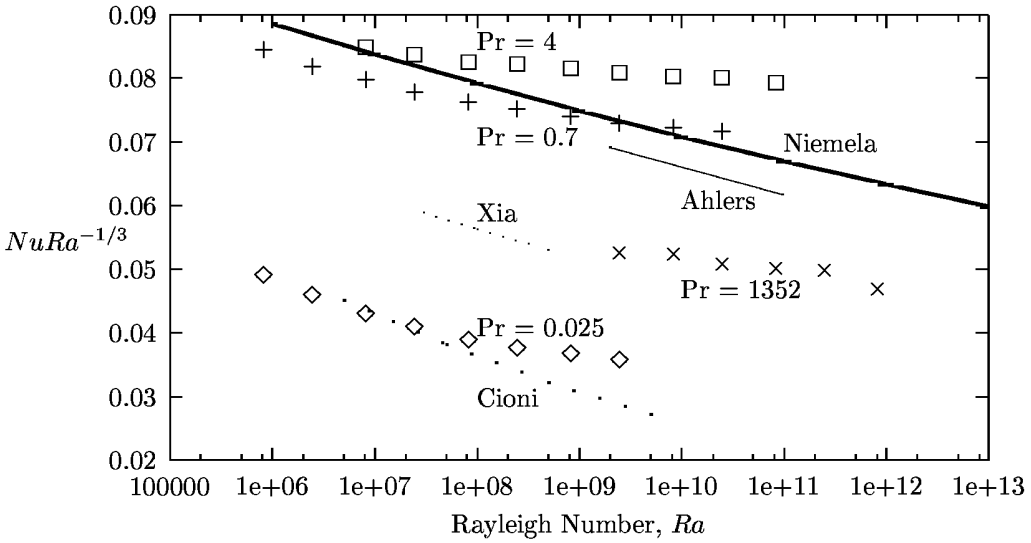

FIG. 3. Nu as a function of Ra for $ZC^2 = 10^4$ and $C^2 = 1200$. Symbols are ODT simulation results for $Pr = 0.025$ (diamonds), $Pr = 0.7$ (crosses), $Pr = 4$ (boxes) and $Pr = 1352$ (×'s). Lines are reported fits to experimental data for $Pr = 0.025$ (Cioni *et al.* 1997), $Pr = 0.7$ (Niemela *et al.* 2000), $Pr = 4$ (Ahlers & Xu 2002, without side-wall heat loss correction), and $Pr = 1352$ (Xia *et al.* 2002).

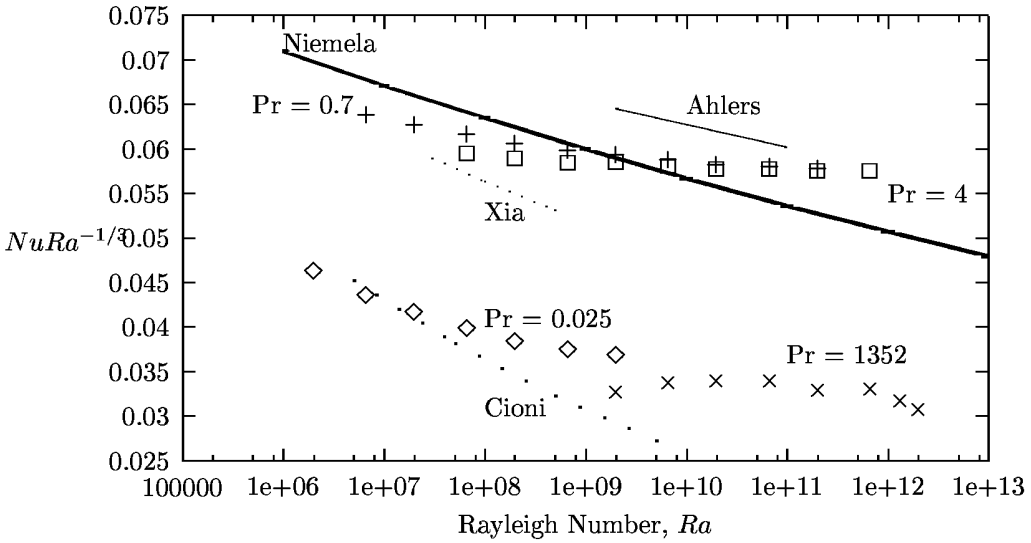

FIG. 4. Nu as a function of Ra for $ZC^2 = 10^5$ and $C^2 = 1500$. Symbols are ODT simulation results for $Pr = 0.025$ (diamonds), $Pr = 0.7$ (crosses), $Pr = 4$ (boxes) and $Pr = 1352$ (×'s). Lines are reported fits to experimental data for $Pr = 0.025$ (Cioni *et al.* 1997), $Pr = 0.7$ (Niemela *et al.* 2000, as corrected for side-wall heat loss by Ahlers & Xu 2002), $Pr = 4$ (Ahlers & Xu 2002, with side-wall heat loss correction), and $Pr = 1352$ (Xia *et al.* 2002).

For $ZC^2 = 10^4$ (Fig. 3), the ODT data agree very well with the mercury convection data of Cioni *et al.* (1997), with the largest discrepancy being only about 15%. The $Pr = 0.7$ matches the helium data of Niemela *et al.* (2000) to within 5%, and the high Prandtl number case plausibly matches the data of Xia *et al.* (2002), although the range of Rayleigh numbers do not overlap. However, the ODT Nu values for $Pr = 4$ consistently exceed those of Ahlers &

Xu (2002) by about 25%. The experimental data shown in figure 3 neglect the side-wall heat-loss model proposed by Ahlers & Xu (2002), which would lower the experimental Nu values even further.

In Figure 4, ODT data for $ZC^2 = 10^5$ are compared to data from the same experiments as in Figure 4. However, the data from Ahlers & Xu (2002) is shown with correction from the side-wall heat-loss model, and the data from Niemela *et al.* (2000) is also shifted downward according to this correction as suggested by Ahlers & Xu (2002). This is done to allow a consistent comparison, and is not meant to imply that either choice is necessarily correct. For this larger value of ZC^2, the model data at low Prandtl number exhibit a larger scaling exponent of Nu with Ra than is seen for $ZC^2 = 10^4$ or in the data of Cioni *et al.* (1997). These results are closer to the experimental data of Takeshita *et. al.* (1996), however (not shown). The data for $Pr = 0.7$ and $Pr = 4$ are also closer to the classical scaling of $1/3$, but differ from the experimental data by less than 10% despite the difference in scaling exponents. The $Pr = 1352$ data exhibits approximately classical scaling and is lower than the extrapolated results of Xia *et al.* (2002) by about 50%. Overall, it is seen that increasing ZC^2, in addition to shifting the peak of the $Nu(Pr)$ curve in figure 2, also results in $Nu(Ra)$ scaling which is closer to the classical value $1/3$ over the range of Ra simulated.

Figures 2-4 demonstrate that ODT reproduces the qualitative trends observed in convection cell experiments. Quantitative agreement depends on the interpretation of side-wall heat loss and the effects of aspect ratio, which are not represented in the model. Hence it is not possible to determine if there exists a particular choice of parameters C and ZC^2 for which the model would correctly reproduce $Nu(Ra, Pr)$ in an infinite-aspect-ratio system. However, the values of Nu produced by the model are adequate for study of the core fluctuations, which requires only that the heat transfer rate approximate the physical value for a given choice of the Rayleigh and Prandtl numbers.

B. Core Density Fluctuations

In the ODT simulations, a significant density gradient is observed in the core of the convection cell. The presence of a density gradient (on average) in experimental cells has not been confirmed or ruled out (to our knowledge). Its appearance in the model simulations is explained using a simple flux-balance argument.

Assuming a constant density gradient across the core region, the average density $\langle \delta\rho(y) \rangle$ is expressed in the form

$$\frac{\langle \delta\rho(y) \rangle}{\Delta\rho} = \frac{1}{2} + \alpha \left(\frac{y}{\Lambda} - \frac{1}{2} \right) \tag{25}$$

which defines the dimensionless gradient α as the ratio of the average gradient in the core to the mean gradient $\Delta\rho/\Lambda$. The core gradient can be quite substantial, often exceeding $\alpha \sim 0.1$ for low values of Ra and Pr.

The magnitude of the core density gradient α is estimated by considering the transport properties of the interior. The density flux (proportional to heat flux) F through the core is estimated for eddies comparable in size to the cell height Λ (these largest eddies dominate transport) as

$$F \sim \frac{\Lambda}{\tau_\Lambda} \alpha \Delta\rho \tag{26}$$

where τ_Λ is the eddy turnover time and $\alpha\Delta\rho$ is the typical density variation across the core of the cell. Assuming this density difference is the driving force behind this transport, the typical turnover time is $\tau_\Lambda \sim \left(gC^2 \alpha \Delta\rho / \Lambda \rho_o \right)^{-1/2}$. The flux is then

$$F \sim \frac{\kappa \Delta\rho}{\Lambda} \alpha^{3/2} \left(RaC^2 Pr \right)^{1/2}. \tag{27}$$

This flux must balance the flux at the wall, given by $F \sim Nu\, \kappa \Delta\rho / \Lambda$. Enforcing this balance yields

$$\alpha \sim \left(\frac{Nu^2}{RaC^2 Pr} \right)^{1/3}. \tag{28}$$

Figure 5 demonstrates this correlation using values of α determined by fitting the average density profile in each ODT simulation to a line in the middle 3/4 of the cell. The correlation is independent of the value of ZC^2, which is expected since (28) is based on large-scale transport. The value of C does matter, since this parameter sets the large eddy turnover rate and hence the overall heat transfer.

The larger values of the core density gradient ($\alpha \geq 0.1$) shown in figure 5 occur at low Pr. The high molecular diffusivity in these cases generates a large flux at the wall, which must be balanced in the core by turbulent transport

along a large density gradient. At low Pr, the large value of α probably influences the dynamics of the thermal boundary layers and consequently plays a role in the observed non-classical scaling of Nu with Ra.

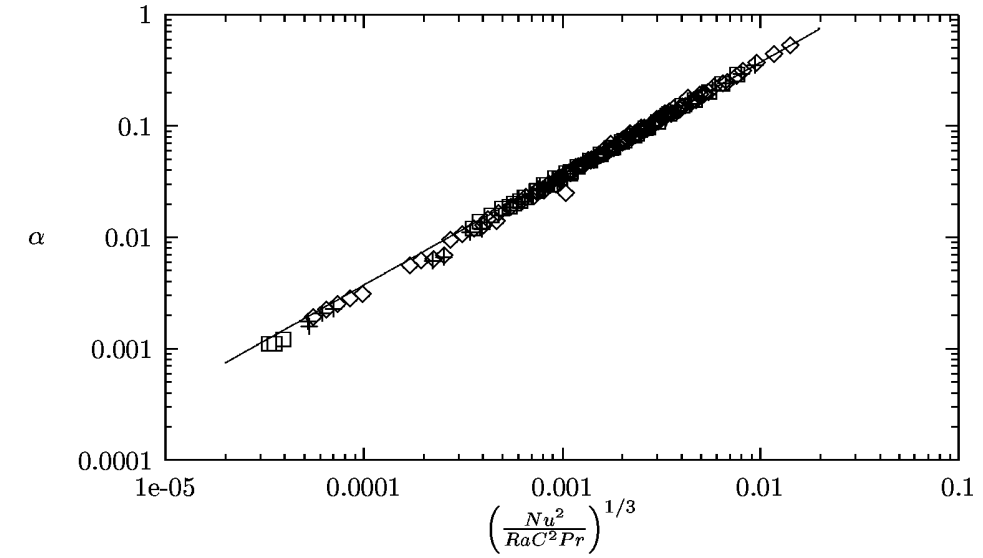

FIG. 5. Magnitude of the core density gradient. Symbols are ODT simulation results for three different values of ZC^2: $ZC^2 = 823$ (diamonds), $ZC^2 = 10^4$ (crosses), and $ZC^2 = 10^5$ (squares). The line is $\alpha = 37.4 \left(\frac{Nu^2}{RaC^2Pr}\right)^{1/3}$.

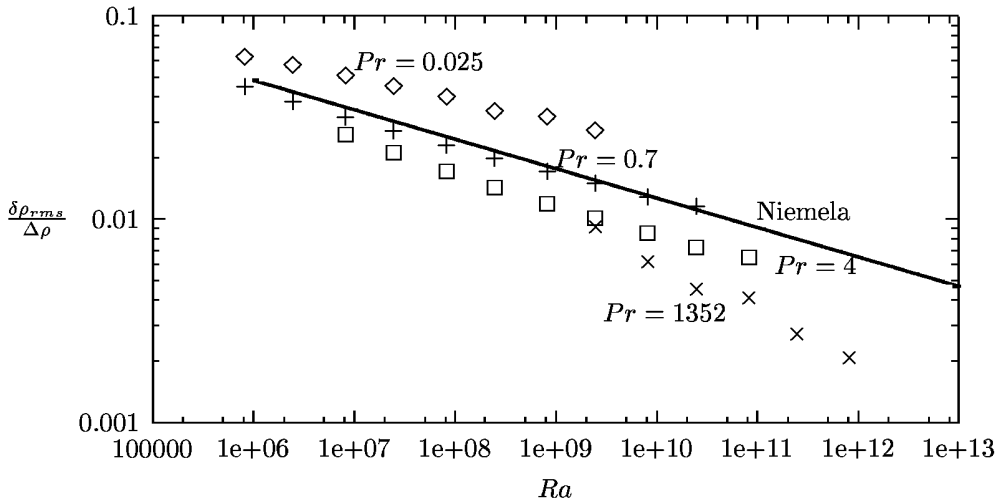

FIG. 6. Magnitude of density fluctuations in the interior. Symbols are ODT simulation results for $ZC^2 = 10^4$ at $Pr = 0.025$ (diamonds), $Pr = 0.7$ (crosses), $Pr = 4$ (squares) and $Pr = 1352$ (×'s); line is a reported fit to $Pr = 0.7$ experimental data (Niemela *et al.* 2000).

Figure 6 shows the magnitude of the density fluctuations observed in the core of the cell for the representative cases presented in figures 3-4. In this study the fluctuations $\delta\rho_{rms}$ are defined as the root-mean-squared (rms) deviations from the average density profile, and the 'core' is defined as the middle 1/4 of the cell. This definition eliminates the spatial variability due to the mean density gradient, making the data comparable to experimental data taken at a single point. Because $\delta\rho_{rms}$ is normalized by the density jump $\Delta\rho$ across the cell, it is directly comparable to experimentally measured temperature fluctuations (normalized by the temperature difference across the cell) if the density and temperature are linearly related (as is commonly assumed). The experimentally observed temperature fluctuation magnitude for helium ($Pr = 0.7$) is also shown (Niemela *et al.* 2000), and the agreement with the ODT

data for $ZC^2 = 10^4$ is excellent (errors less than 10%) at this Prandtl number. (It is worth noting that this value of ZC^2 also gave the best agreement with the corresponding Nusselt-number data.)

The Pr dependence of ODT results for $\delta\rho_{rms}$ which is evident in figure 6 is further illustrated in figure 7. For any given ZC^2, there is a minimum value of $\delta\rho_{rms}$ which occurs at $Pr \sim 200$ for $ZC^2 = 823$ but shifts to $Pr \sim 50$ for $ZC^2 = 10^4$ and $Pr \sim 20$ for $ZC^2 = 10^5$. Figure 7 also shows that $\delta\rho_{rms}$ depends only weakly on ZC^2 at low Prandtl number. For comparison, experimental values for helium (Niemela *et al.* 2000) and water solutions at several Prandtl numbers at a larger Ra value (Daya & Ecke 2002) are also shown. Again, the helium data compare favorably to the ODT simulations, and the water solutions exhibit the same trend with Pr although the absolute magnitude is smaller by a factor of approximately 2.

Estimation of the Ra-scaling of the ODT core density fluctuations $\delta\rho_{rms}$ for many values of Pr indicated that the scaling exponent exhibits a strong dependence on the Prandtl number. (Simulations at $Ra = 10^8$ and $Ra = 10^9$ were used to calculate the scaling exponents.) At the smallest Prandtl number simulated ($Pr = 0.025$), the scaling exponent is approximately -0.11. It increases slowly until Pr reaches the value corresponding to the minimum in figure 7 (a value which varies slightly with ZC^2), and then rises rapidly up to -0.3 for $Pr = 1352$. These scaling exponents show only weak dependence on the value of ZC^2. For $Pr = 0.7$, the ODT value of -0.13 compares favorably to the experimental values of -0.145 (Niemela *et al.* 2000) and -0.147 ± 0.005 (Castaing *et al.* 1989). For $Pr = 5.5$, Daya & Ecke (2001) report an exponent of -0.10 ± 0.02, which is smaller in magnitude than the model exponent of -0.15. Daya & Ecke (2002) also report that the magnitude of the scaling exponent increases as Pr increases, up to -0.18 for $Pr = 10$ (compared to -0.17 for ODT at $Pr = 10$). Thus, the ODT exponents follow the trend found by Daya & Ecke (2002) although the dependence on Pr is somewhat weaker.

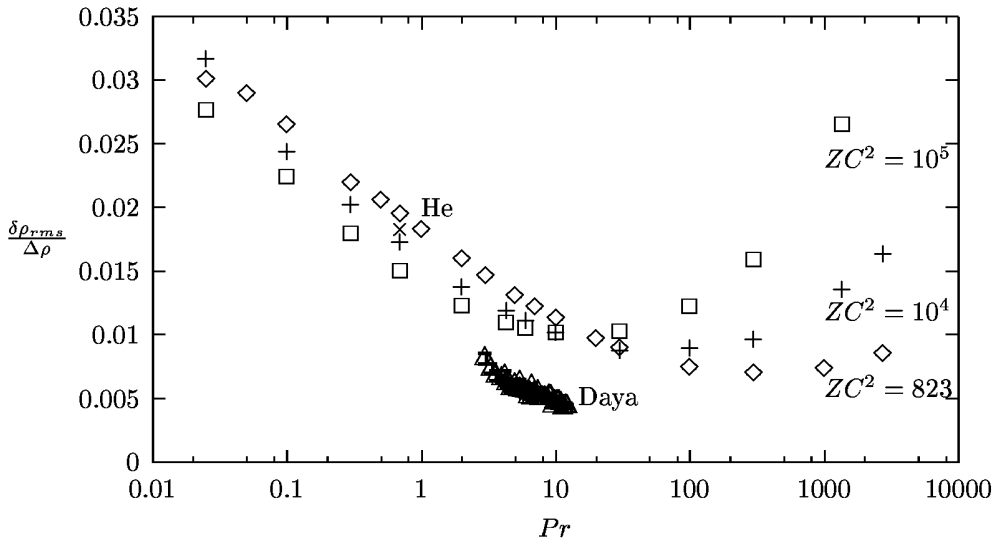

FIG. 7. Magnitude of density fluctuations in the interior as a function of Pr at $Ra = 10^9$. Diamonds are ODT data for $ZC^2 = 823$, crosses are for $ZC^2 = 10^4$, and squares are for $ZC^2 = 10^5$. Experimental data for helium (He) at the same Rayleigh number is also shown (×'s) (Niemela *et. al.* 2000), as is experimental data for water solutions at a number of Pr values for $Ra = 2 \cdot 10^9$ (triangles) (Daya & Ecke 2002).

A simple picture of the density fluctuations yields a crude estimate of the Ra and Pr dependence of $\delta\rho_{rms}$. In this view, there are two distinct sources of core density fluctuations. One is the mixing of the core density gradient by eddies, whose contribution to the rms core density fluctuations is labelled $\delta\rho^2_{core}$; and the other is the transport of fluid elements from the thermal boundary layers directly to the core region by plumes which reach the core with minimal diffusive mixing; this contribution is labelled $\delta\rho^2_{BL}$. Assuming that these two contributions are statistically independent, the total rms density fluctuation is given by

$$\delta\rho^2_{rms} = \delta\rho^2_{core} + \delta\rho^2_{BL}. \tag{29}$$

The contribution $\delta\rho^2_{core}$ due to the core fluctuations is proportional to $(\alpha\Delta\rho)^2$ (where α is given by (28)), since this is the total density variation across the core region. Estimating the boundary-layer contribution requires an understanding of the frequency with which large eddies (the ODT equivalent of plumes) transport a substantial fraction of the boundary layer directly into the core region. Each eddy transports a 'blob' of fluid whose width scales

as Λ/Nu (the boundary layer thickness) with a density fluctuation of order $\Delta\rho$. These blobs appear in the core region with some frequency τ_b^{-1} and survive in the core for some lifetime $\tau_l \ll \tau_b$. Their total contribution to the density fluctuations is

$$\delta\rho_{BL}^2 \sim \Delta\rho^2 Nu^{-1}\,(\tau_l/\tau_b) \tag{30}$$

based on a space-time average over many blobs. The typical frequency τ_b^{-1} is estimated from the energy released when a blob with mass on the order of $\Lambda\Delta\rho/Nu$ is transported a distance of order Λ:

$$\tau_b^{-1} \sim \sqrt{\frac{g\Delta\rho}{Nu\rho_o\Lambda}}. \tag{31}$$

The lifetime τ_l of the blob in the turbulent core is more difficult to determine, but a plausible estimate is to use the turnover time of the smallest (Kolmogorov-scale) eddies. This assumes that the typical blob which breaks off from the thermal boundary layer is smaller than the Kolmogorov scale, an assumption which has been verified in ODT for larger Prandtl numbers ($Pr \geq 1$). Therefore the smallest eddies are the relevant ones for blob break-up and dissipation. The blob lifetime therefore scales as $\tau_l \sim (\Lambda^2/\nu)Re^{-3/2}$, where Re is the Reynolds number. It is shown in Section IV.C that Re in the core of the cell scales as $Re^3 \sim RaNuPr^{-2}$. Combining these time scales yields

$$\delta\rho_{BL}^2 \sim \Delta\rho^2 \frac{Pr^{1/2}}{Nu^2} \tag{32}$$

for the boundary layer contribution, and an overall expression for $\delta\rho_{rms}$ of

$$\left(\frac{\delta\rho_{rms}}{\Delta\rho}\right)^2 = A\left(\frac{Nu^2}{RaC^2Pr}\right)^{2/3} + B\frac{Pr^{1/2}}{Nu^2} \tag{33}$$

where A and B are constants. In the limit $Pr \to 0$, the core gradient is large and the boundary layer contribution to $\delta\rho_{rms}$ is negligible. This yields the classical result $\delta\rho_{rms} \sim \Delta\rho(RaPr)^{-1/9}$ if $Nu \sim (RaPr)^{1/3}$ (Siggia 1994). This is comparable to the observed ODT Rayleigh number scaling exponent of -0.11 in the $Pr = 0.025$ case. In the other limit, $Pr \to \infty$, the core gradient vanishes and the boundary layer contribution increases until it dominates the fluctuations. In this case $\delta\rho_{rms} \sim \Delta\rho Ra^{-1/3}$ (assuming $Nu \sim Ra^{1/3}$), which is consistent with the value -0.3 inferred from the $Pr = 1352$ ODT data. Intermediate values of Pr yield exponents that lie between these limits, since the sum of two scaling functions with distinct exponents mimics a scaling function with an intermediate exponent value. For fixed Pr, the core term always dominates in the limit $Ra \to \infty$ (assuming the $Nu(Ra)$ scaling exponent exceeds $1/5$). The fluctuation magnitude estimate of (33) also produces a minimum at a Pr value where both terms contribute substantially to the total, which is consistent with the ODT data shown in figure 7.

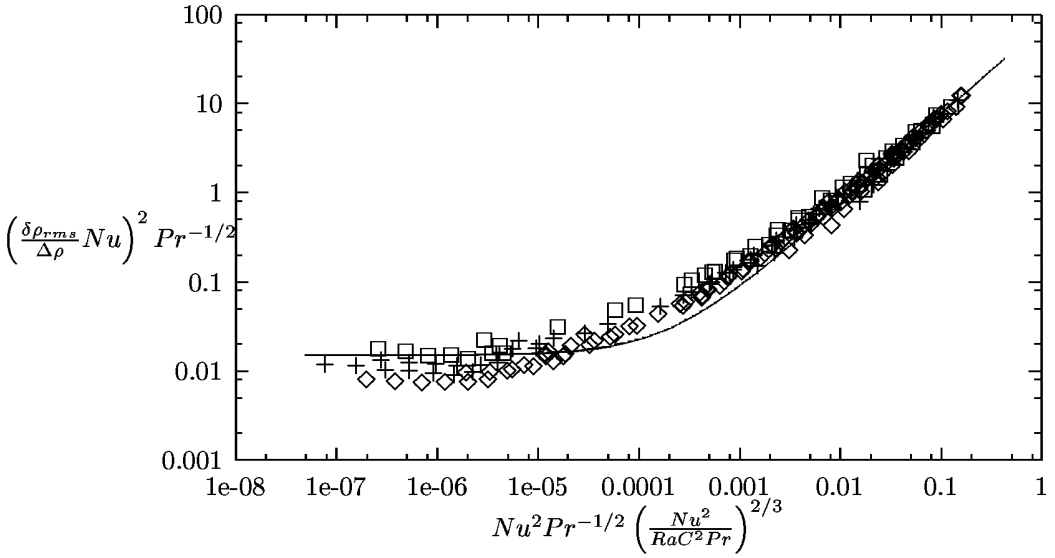

FIG. 8. Scaling of the density fluctuations, as suggested by a simple model with two sources of fluctuations. Diamonds are ODT simulation data for $ZC^2 = 823$, crosses are for $ZC^2 = 10^4$, and squares are for $ZC^2 = 10^5$, while the line is a fit of (33) with $A = 75$ and $B = 0.015$.

Figure 8 illustrates the scaling suggested by (33) for all of our ODT simulation data. The results are shown on a logarithmic scale since the normalized density fluctuations vary over several orders of magnitude. This illustrates the parameter regime where the core contribution dominates (upper right portion of figure 8) as well as the regime where the boundary layer dominates and $\left(\frac{\delta\rho_{rms}}{\Delta\rho}Nu\right)^2 Pr^{-1/2}$ is approximately constant (lower left portion of figure 8). The line shows a fit of (33) to the data. However, while the same value of A matches all three values of ZC^2, it is clear from figure 8 that slightly different values of B would best match the data for each value of ZC^2. Hence, although the core contribution to $\delta\rho_{rms}$ appears to be independent of ZC^2, the boundary layer contribution apparently increases as ZC^2 increases. Figure 8 shows that, although (33) gives good agreement with the ODT data in the limiting cases where either the core or boundary layer contributions dominate, it is imperfect in the portion of parameter space where both are significant. The assumption of statistical independence of the two contributions is probably at least partially responsible for this error. However, even at its worst, the estimate of (33) is within 40% of the ODT results, which is not bad considering that $\delta\rho_{rms}$ varies by over two orders of magnitude.

It is worth recognizing that the separation of the density fluctuations into two distinct sources is somewhat artificial, since it is obvious that all fluctuations must ultimately originate in the thermal boundary layers. It is perhaps better to think of the contribution of the core density gradient as representing the effects of fluid elements which interact significantly with their environment while transiting from the boundary layer to the cell center (producing the average density gradient), while the explicit boundary-layer contribution to (33) represents the effects of plumes which reach the cell center with minimal interaction. In ODT, the difference between these two mechanisms arises because fluid elements may transit from boundary layer to cell center either indirectly, as a result of a large number of eddy mappings (allowing some equilibration with the environment along the way) or directly as a result of only one or two mappings (allowing little time for equilibration).

To study the statistics of the density fluctuations in the core of the cell, we collected density values in narrow spatial intervals 1/64th of the cell height Λ in length. Figure 9 shows the probability distribution function (pdf) of density values observed at the center of the cell, normalized by $\delta\rho_{rms}$ (the square root of the pdf variance), for $Pr = 5.5$ and $Ra = 2 \cdot 10^9$. Results for all three values of ZC^2 are shown. Generally, ODT pdf shapes do not appear to depend on the value of ZC^2 except when extreme fluctuations (ten or more standard deviations) are considered. The pdf shape is approximately exponential out to at least 6 standard deviations. Experimental data (Daya & Ecke 2001) for the same Ra and Pr are also shown in figure 9, and the pdf shapes are nearly identical. Interestingly, this data was collected in two different geometries - a cylindrical cell and a square cell - yet the pdf shapes match each other and ODT. However, the values of $\delta\rho_{rms}$ used to normalize the pdfs are different in all three cases. Hence it seems that, while the value of $\delta\rho_{rms}$ may depend strongly on geometry, the pdf shape is more universal and is correctly generated by ODT. This suggests that the physical mechanism which detemines the shape is relatively simple and accessible to the model.

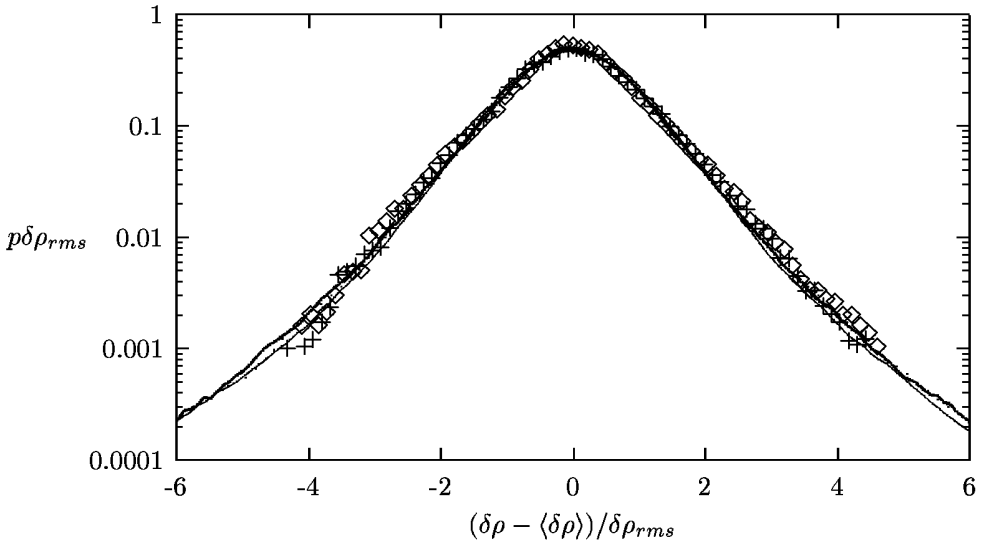

FIG. 9. Rescaled pdf p of ODT core density fluctuations (lines) for $Pr = 5.5$, $Ra = 2 \cdot 10^9$, and all three values of ZC^2. Here $\langle\delta\rho\rangle = 0.5\Delta\rho$ and $\delta\rho_{rms}^2$ is the variance of the pdf. For comparison, experimental data in two distinct cell geometries (diamonds for cylindrical geometry, crosses for square geometry) with the same Ra and Pr are also shown (Daya & Ecke 2001).

It was recognized in the helium convection experiments of Castaing *et al.* (1989) that the universal shape of the pdf when normalized by $\delta\rho_{rms}$ applies over a wide range of Rayleigh numbers. Figure 10 illustrates this collapse for $Pr = 0.7$ for four values of Ra spanning three orders of magnitude. The results for $ZC^2 = 10^5$ are shown here and in subsequent figures because more statistics were collected for those simulations than for smaller values of ZC^2, but as previously noted (see figure 9) the shape does not depend on ZC^2 over the range of fluctuations shown. Again, the simulation pdfs are well approximated by an exponential form within 6 standard deviations of zero. The experimental data of Castaing *et al.* (1989) are also shown in figure 10 for comparison. To facilitate a direct comparison, histogram data from their paper was digitized and normalized to produce the approximate pdfs shown in figure 10. While there is excellent agreement for negative fluctuations, the experimental pdf exhibits an asymmetry which the (inherently symmetric) model does not have.

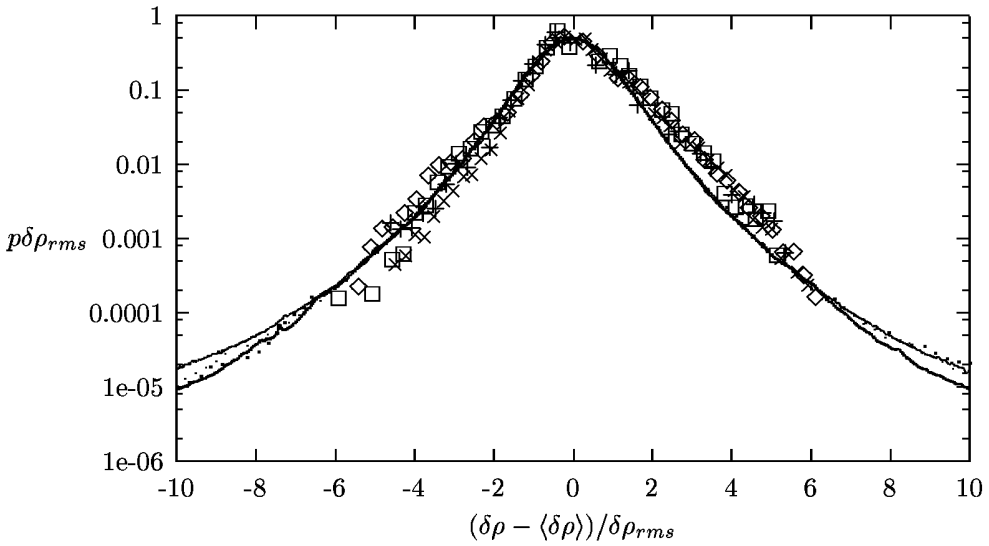

FIG. 10. Rescaled pdfs p of ODT core density fluctuations for $Pr = 0.7$ and $ZC^2 = 10^5$ using the same normalization as in figure 9. Four distinct Ra values ($Ra = 2 \cdot 10^7$, $2 \cdot 10^8$, $2 \cdot 10^9$, and $2 \cdot 10^{10}$) are shown, but the shapes are indistinguishable to 6 standard deviations. For comparison, experimental data (symbols) for helium convection (Castaing *et al.* 1989) is also shown for four Ra values between 10^8 and 10^{12}.

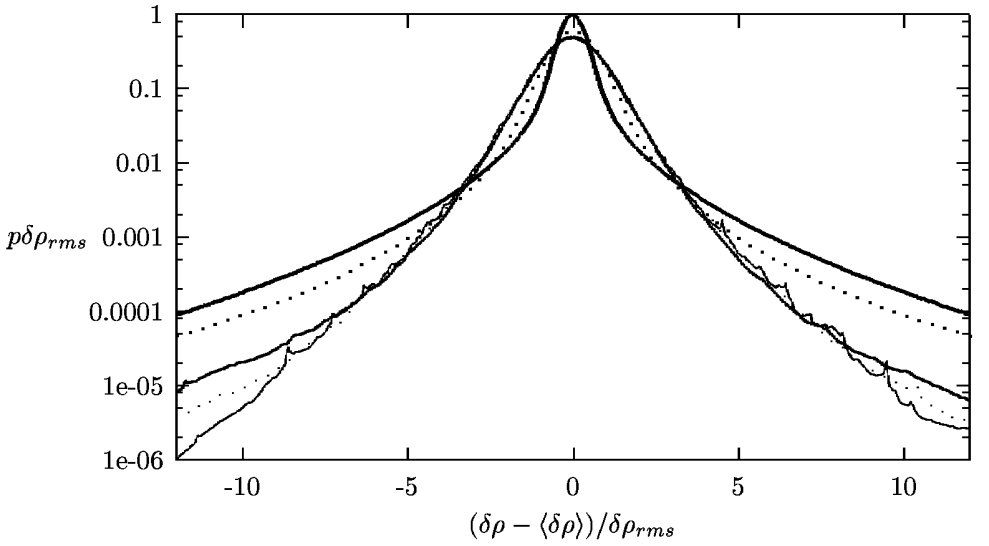

FIG. 11. Rescaled pdfs p of core density fluctuations for $Ra = 2 \cdot 10^9$, $ZC^2 = 10^5$, and five Pr values: 0.1, 0.7, 4, 100, and 1352. The rescaled probability of large fluctuations increases with Pr.

The collapse of the pdfs must ultimately fail at large deviations because $|\delta\rho - \langle\delta\rho\rangle|$ is bounded by $0.5\Delta\rho$ due to the finite cell size. This breakdown is observed in ODT as a long, non-exponential tail in the pdf followed by the truncation of the pdf at $|\delta\rho - \langle\delta\rho\rangle| = 0.5\Delta\rho$. The separation of the pdfs is seen in figure 10 beginning at approximately 8 standard deviations.

The collapse of the pdf cores illustrated in figures 9 and 10 is tested for different Pr values (at fixed Ra) in figure 11. Although the low-Pr case is more noisy than the others, the $Pr = 0.1$, $Pr = 0.7$, and $Pr = 4$ pdfs appear to overlap within five standard deviations of the average density value. At very large deviations the pdfs progressively diverge from each other, with the probability of very large deviations increasing with Pr. However, the $Pr = 100$ and $Pr = 1352$ simulations exhibit sharper pdf cores and do not match the others. Hence it appears that the collapse of the pdfs proposed by Castaing *et al.* (1989) does not apply to high-Pr data in the ODT model.

The fact that the rescaled pdf shape appears to be independent of Ra and Pr for $Pr < 100$ indicates that the same mechanism is operative over this wide range of parameter values. Based on the previous analysis of the magnitude of the density fluctuations which led to (33), this shape is apparently the result of the transport of fluid elements from boundary layer to core via the 'indirect transport' (or core gradient) process in which a fluid element interacts significantly with its environment while passing from boundary layer to cell center. This is inferred because this contribution dominates the estimate of $\delta\rho_{rms}$ at low Pr values in (33). The transition to a different pdf shape at larger Pr values is seen in simulations in which the 'direct transport' mechanism, in which plumes move from boundary layer to cell center without much equilibration with their environment during transit, becomes the dominant contribution to $\delta\rho_{rms}$ in (33). Hence the two distinct pdf shapes are apparently indicative of the two distinct contributions to the magnitude of the density fluctuations $\delta\rho_{rms}$. This analysis suggests that observations of the pdf in high-Pr convection experiments, such as those of Xia *et al.* (2002), might reveal a different shape than has been previously seen experimentally.

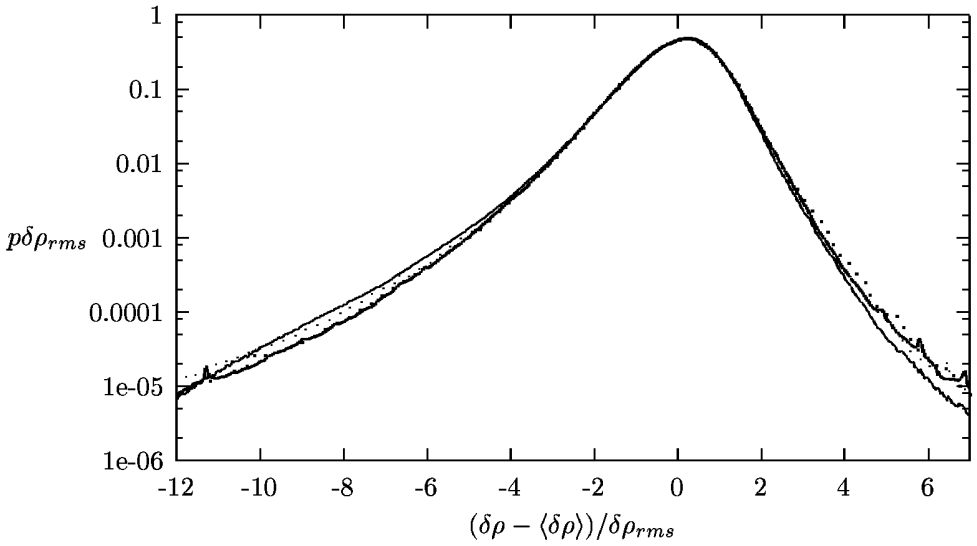

FIG. 12. Rescaled off-center pdfs of core density fluctuations for $Pr = 0.7$, $ZC^2 = 10^5$, and Ra values of $2 \cdot 10^7$, $2 \cdot 10^8$, $2 \cdot 10^9$, and $2 \cdot 10^{10}$. The position is $y = \Lambda/4$.

Figure 12 shows the pdfs of density values at the off-center location $y = 0.25\Lambda$ for the same $Pr = 0.7$ simulations as figure 10. Again the results are normalized by the rms value of the density fluctuations. Since the location lies closer to the bottom of the cell (where $\delta\rho = 0$) than to the top (where $\delta\rho = \Delta\rho$), it is not surprising that negative values of $\delta\rho$ are much more frequent than positive values. Long tails which vary slightly with Ra are evident on the left side of the pdf, with larger Ra giving a higher probability of large negative deviations. The right side of the pdf falls off much more steeply than the pdf in the cell center (see figure 10). Apparently, the increased distance from the upper boundary layer (compared to the cell center pdf) results in a faster decrease in the pdf. To our knowledge there are no published experimental data on off-center density fluctuation pdfs for comparison with the model data. Off-center pdfs at $y = 0.75\Lambda$ (not shown) are approximately a mirror image of figure 12, as expected.

Off-center pdfs (at $y = 0.25\Lambda$) for 5 different Prandtl numbers are shown in figure 13. As in figure 11, the large-Pr and small-Pr pdfs exhibit two distinct shapes at small standard deviations. Also, there is a higher probability of large-deviation events at higher Pr. The asymmetry due to the proximity to the lower cell boundary is again evident.

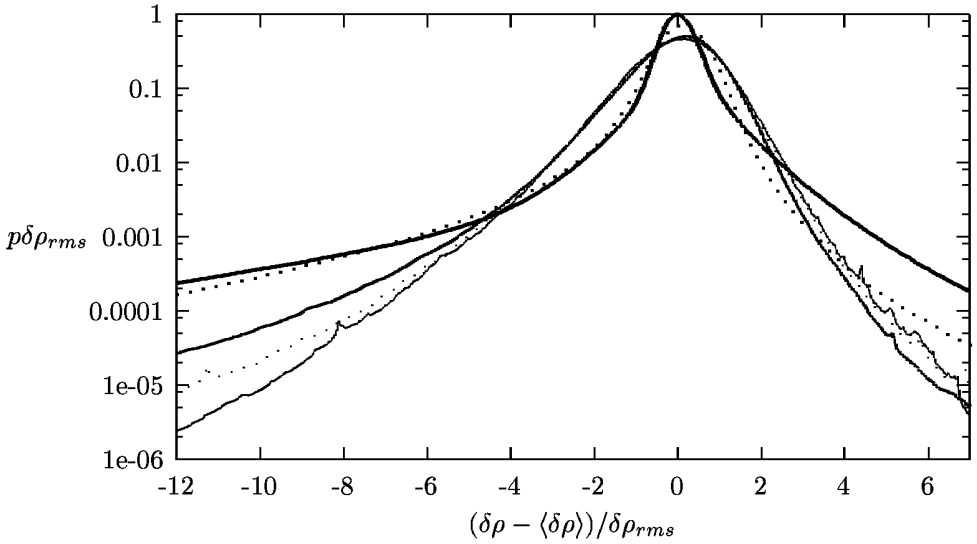

FIG. 13. Rescaled off-center pdfs of core density fluctuations for $Ra = 2 \cdot 10^9$, $ZC^2 = 10^5$, and five values of Pr: 0.1, 0.7, 4, 100, and 1352. The probability of large negative fluctuations increases with Pr, as in figure 11.

C. Core velocity fluctuations

The magnitude of the ODT 'velocity' fluctuations in the core of the cell can be estimated using energy conservation (14) and the characteristics of the turbulent cascade, which the model mimics by design in the absence of a density gradient. Because the density is nearly constant in the core of the cell, the turbulent cascade operates with little interference in most of the cell. It is therefore plausible to estimate the energy dissipation based on the cell size Λ and the typical velocity scale U in the cell core. The energy input to the cascade at the large scale is U^3/Λ; balancing this against the dissipation (assuming a steady cascade) implies

$$\frac{U^3}{\Lambda} \sim \nu\langle(\partial_y v)^2\rangle. \tag{34}$$

The dimensionless energy dissipation ϵ is therefore

$$\epsilon \equiv \frac{\Lambda^3}{\nu^2}\int \langle(\partial_y v)^2\rangle dy \sim \frac{U^3\Lambda^3}{\nu^3} \equiv Re^3 \tag{35}$$

where $Re \equiv U\Lambda/\nu$ is the Reynolds number. To establish a quantitative relationship, the velocity scale U is defined as $U \equiv \sqrt{\langle v^2\rangle}$, where the average is taken over the middle $1/4$ of the cell (to avoid wall effects) and over the time history of the simulation. Hence the ODT Re is a measure of the rms velocity fluctuations in the core. Using this definition, the proportionality between Re^3 and energy dissipation ϵ is obeyed in the ODT simulations to within a few percent.

A corollary of this scaling, due to the energy conservation equation (14), is a relationship between the magnitude of the velocity fluctuations Re and the heat transfer Nu:

$$RePr = 1.4C^{-1/3}\left(RaPr(Nu-1)\right)^{1/3} \tag{36}$$

with the constant of proportionality, $1.4C^{-1/3}$, determined by fitting the simulation data for all values of ZC^2. This relation is demonstrated for the ODT simulations in figure 14. Hence, by combining energy conservation with the assumption of a turbulent cascade, a non-trivial relationship (36) for the magnitude of the velocity fluctuations has been obtained, in agreement with the ODT simulation data.

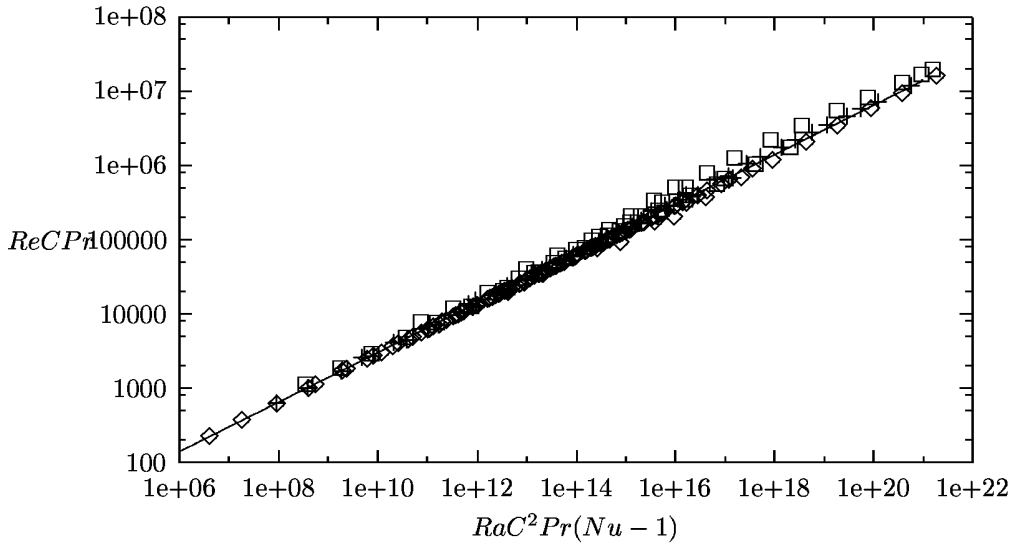

FIG. 14. The energy conservation relation (36) giving the magnitude of the (non-dimensionalized) core velocity fluctuations Re. Symbols are simulation results for $ZC^2 = 823$ (diamonds), $ZC^2 = 10^4$ (crosses), and $ZC^2 = 10^5$ (boxes). The dotted line is (36).

A few experiments have attempted to measure velocity fluctuations and estimate Re in the convection cell. Using published scaling estimates for Re and Nu, the experimental results for different Prandtl numbers are given approximately by:

$$RePr = (RaPrNu)^{1/3} \times \begin{cases} 2.1\left(10^{-9}Ra\right)^{0.004} & (Pr = 0.025,\ 5\cdot 10^6 \le Ra \le 5\cdot 10^9) \\ 1.9\left(10^{-9}Ra\right)^{0.057} & (Pr = 0.7,\ \ 10^8 \le Ra \le 10^{14}) \\ 2.0 & (Pr = 7,\ \ 3\cdot 10^7 \le Ra \le 4\cdot 10^9) \end{cases} \tag{37}$$

The liquid mercury data ($Pr = 0.025$) are taken from Cioni *et al.* (1997); the helium data ($Pr = 0.7$) are from Castaing *et al.* (1989), and the water ($Pr = 7$) data from Tanaka & Miyata (1980). These experimental results do not all scale identically to the ODT relation (36), but the deviations only amount to a few percent in Re over three orders of magnitude in Ra in the worst case. The experimentally determined constants in the scaling relations indicate that the ODT Re values are about 1/5th of the experimental values (for $C^2 \sim 10^3$), which is not bad considering the ambiguities inherent in defining the ODT velocity magnitude U. These experimental results indicate no significant dependence of the prefactor on Prandtl number at $Ra = 10^9$.

The Prandtl-number dependence of Re has been studied in a single apparatus using a variety of fluids to cover the range $3 \le Pr \le 1205$ (Lam *et al.* 2002). Based on the rms fluctuations of the velocity magnitude in the core, they report that $Re = 0.84Ra^{0.40\pm0.03}Pr^{-0.86\pm0.01}$. Combining this with $Nu = 0.14Ra^{0.3}Pr^{-0.03}$ measured in the same apparatus (Xia *et al.* 2002) gives

$$RePr \simeq 3.2Pr^{-0.18}\,(RaPrNu)^{1/3} \tag{38}$$

which indicates the prefactor in (36) decreases slowly with Pr, in contrast to the ODT data. However, the experimental Rayleigh numbers at $Pr \simeq 10^2$ to 10^3 are much lower than those simulated by ODT, and may not exhibit a fully-developed cascade. This would violate the assumptions that led to (36), and hence at higher experimental Ra it is possible that this Pr dependence may weaken and the results become more similar to those of ODT.

The pdf of fluctuations in the value of the ODT 'velocity' scalar in the center the cell is shown in figure 15, along with the only experimental data (for vertical velocity fluctuations) of which we are aware (Daya & Ecke 2001). The data is for $Pr = 5.5$ and $Ra = 2\cdot 10^9$, and was collected in both a cylindrical and a square cell (as were the density pdfs shown in figure 9). As was the case for the density fluctuations, the magnitude of the rms velocity fluctuation U used to scale the pdfs is different for the two geometries and for ODT, but the shape of the rescaled pdf appears to be more universal. Off-center velocity fluctuation pdfs (not shown) taken at $y = 0.25\Lambda$ and $y = 0.75\Lambda$ showed no significant dependence of the pdf shape on position within the cell core (in contrast to the density pdfs).

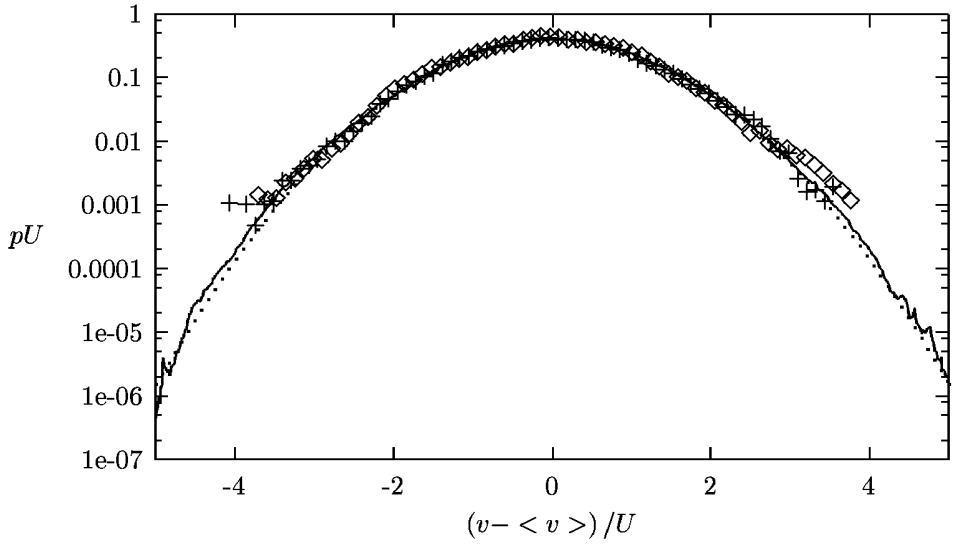

FIG. 15. Rescaled pdf p of core velocity fluctuations. ODT simulation data (solid line) for $Pr = 5.5$, $Ra = 2 \cdot 10^9$, and $ZC^2 = 10^5$. Experimental data from the cell center in two distinct geometries (diamonds for cylindrical geometry, crosses for square geometry) for the same Ra and Pr are shown for comparison (Daya & Ecke 2001). Also shown is a Gaussian pdf (dotted line).

D. Fluctuations in open systems.

To further illustrate the importance of the thermal boundary layers in shaping the core density fluctuation pdf, ODT simulations were also performed with jump-periodic boundary conditions imposed on $\delta\rho$ rather than hard walls. This eliminates the thermal boundary layer entirely, and the simulation corresponds to an infinitely long unstable density gradient. Without walls, there is no natural way to truncate the range of possible eddy sizes in the model, so a largest eddy size equal to the periodicity length Λ was imposed. Simulations with Rayleigh numbers in the range $3 \cdot 10^9 \leq RaC^2 \leq 3 \cdot 10^{12}$ were performed for Prandtl number values $Pr = 0.1$, 1.0, and 10 and $ZC^2 = 10^5$. The resulting pdfs had the same shape in all cases; an example is shown in figure 16. The shape is close to a Gaussian, unlike the pdf which results from the simulation with hard walls, which is shown for comparison. The deviation from the Gaussian pdf is the result of the mixing of a density gradient which extends over many integral scales, as has been observed experimentally by Gollub *et al.* (1991) and Jayesh & Warhaft (1991). This effect has also been seen in stochastic models very similar to the one presented here (Holzer & Pumir 1993, Wunsch 1998), and is arguably a common feature of such models in this configuration (Falkovich, Gawedzki & Vergassola 2001). However, the difference between the model pdf in the open and walled configurations demonstrates that the effect of mixing against the density gradient is negligible when walls are present, since the pdf in the walled configuration is very non-Gaussian even at small deviations and exhibits a much larger probability of large deviations. This comparison illustrates the fact that the pdfs generated by the model for walled cells are determined by the transport of boundary layer fluid into the cell interior, and are not an artifact peculiar to models based on stochastic maps.

Heat transfer in this configuration is determined entirely by the large scales. The heat flux is given by $V\Delta\rho/\Lambda$, where the velocity scale V is given by $V \sim g\Lambda\Delta\rho/\rho$. Combining these yields $Nu \sim RePr \sim \sqrt{RaPr}$. These scalings correspond to the so-called 'ultimate regime' of thermal convection (Kraichnan 1962). The ODT simulation results are summarized by $Nu = 0.0075C\sqrt{RaPr}$ and $RePr = 0.28\sqrt{RaPr}$. For $Pr = 1$, $Nu \sim Ra^{1/2}$ has also been observed in direct numerical simulations of this configuration by Lohse & Toschi (2002).

The magnitude of the density fluctuations $\delta\rho_{rms}$ should be constant, according to (33) with these scalings and $B = 0$. This was not quite true in the simulations, as $\delta\rho_{rms}/\Delta\rho$ slowly decreases with increasing RaC^2 with a scaling exponent of approximately 0.02 ± 0.01. This possibly indicates a weak influence of the molecular parameters (κ or ν) on the magnitude of the density fluctuations.

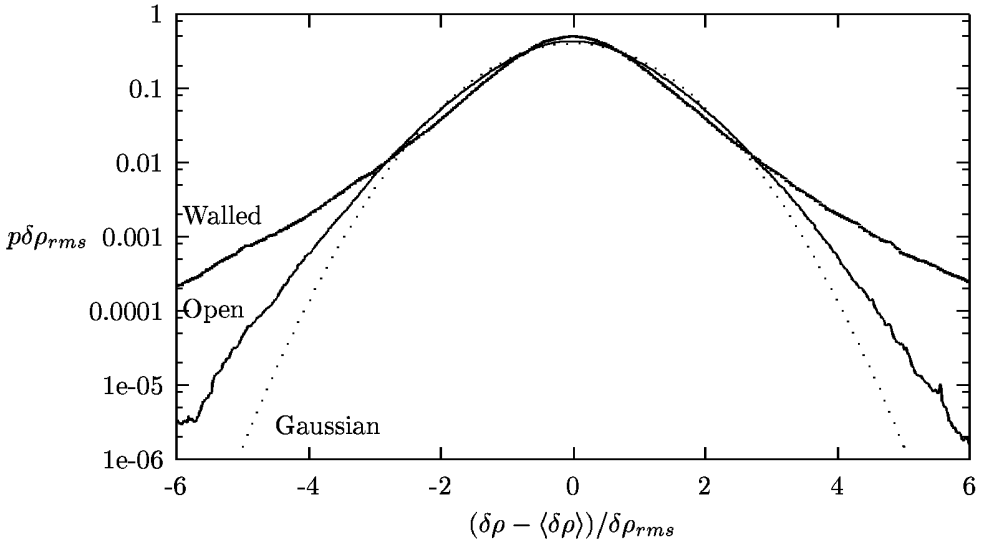

FIG. 16. Rescaled pdf p of density fluctuations in an open (periodic) system, for $RaC^2 = 3 \cdot 10^{12}$, $Pr = 1$, and $ZC^2 = 10^5$. The pdf is very close to a Gaussian (dotted line) but very different from the pdf in a hard-wall simulation with the same parameter values.

V. CONCLUSIONS

In this work, a model based on the stochastic application of a mapping function to a one-dimensional domain, with a dynamical rule based on mixing-length arguments, is applied to turbulent convection. Using only two adjustable parameters, the model approximately reproduces heat-transfer rates measured in Rayleigh-Beńard cells over six orders of magnitude in Ra and five orders of magnitude in Pr. Although the model does not incorporate some effects which are significant in containers with finite horizontal extent, the model can plausibly be used to study interior fluctuations, and might usefully be applied to natural convecting systems (where side-wall effects are unimportant) in the future.

The present study of density (or temperature) fluctuations in the core of a convecting cell demonstrated good agreement between the model and the limited experimental data available for both the overall magnitude of fluctuations and the shape of the fluctuation pdf. However, simulations at larger Prandtl numbers and replacement of the hard walls at the top and bottom with a jump-periodic boundary condition resulted in significant changes to the fluctuation magnitude and pdf. Also, the fluctuation pdf exhibited a strong dependence on vertical location. These results were interpreted using a simple picture in which core fluctuations result from two sources: direct transport of thermal-boundary-layer material into the core with little mixing, and indirect transport, in which boundary-layer material undergoes significant mixing with its surroundings before reaching the core. Changes in the pdf shapes were attributed to shifts in the relative importance of these two mechanisms, and could be observable in large-Pr experiments. Also, a simple mixing-length argument for the scaling of the magnitude of fluctuations was suggested by this picture and shown to be compatible with the model as well as the available experimental data .

ACKNOWLEDGMENTS

We thank Z. Daya and R. Ecke for helpful comments and for sharing their experimental data. This work was supported by the U.S. Department of Energy, Office of Basic Energy Sciences, Division of Chemical Sciences, Geosciences, and Biosciences.

REFERENCES

Ahlers, G. & Xu, X. 2001 Prandtl-number dependence of heat transport in turbulent Rayleigh-Beńard convection. *Phys. Rev. Lett.* **86**, 3320-3323.

Castaing, B., Gunaratne, G., Heslot, F., Kadanoff, L., Libchaber, A., Thomae, S., Wu, X.-Z., Zaleski, S. & Zanetti, G. 1989 Scaling of hard thermal turbulence in Rayleigh-Beńard convection. *J. Fluid Mech.* **204**, 1-30.

Chavanne, X., Chilla, F., Castaing, B. Hebral, B., Chabaud, B. & Chaussy, J. 1997 Observation of the ultimate regime in Rayleigh-Beńard convection. *Phys. Rev. Lett.* **79**, 3648-3651.

Chavanne, X., Chilla, F., Chabaud, B., Castaing, B. & Hebral, B. 2001 Turbulent Rayleigh-Beńard convection in gaseous and liquid He. *Phys. Fluids* **13**, 1300-1320.

Cioni, S., Ciliberto, S. & Sommeria, J. 1997 Strongly turbulent Rayleigh-Beńard convection in mercury: comparison with results at moderate Prandtl number. *J. Fluid Mech.* **335**, 111-140.

Daya, Z.A. & Ecke, R.E. 2001 Does turbulent convection feel the shape of the container? *Phys. Rev. Lett.* **87**, 184501.

Daya, Z.A. & Ecke, R.E. 2002 Prandtl-number dependence of interior temperature and velocity fluctuations in turbulent convection. *Phys. Rev. E* **66**, 045301(R).

Falkovich, G., Gawedzki, K. & Vergassola, M. 2001 Particles and fields in fluid turbulence. *Rev. Mod. Phys.* **73**, 913-975.

Garon, A.M. & Goldstein, R.J. 1973 Velocity and heat transfer measurements in thermal convection. *Phys. Fluids* **16**, 1818-1825.

Goldstein, R.J., Chiang, H.D. & See, D.L. 1990 High-Rayleigh-number convection in a horizontal enclosure. *J. Fluid Mech.* **213**, 111-126.

Goldstein, R.J. & Tokuda, S. 1980 Heat transfer by thermal convection at high Rayleigh numbers. *Int. J. Heat Mass Transfer* **23**, 738-740.

Gollub, J.P., Clarke, J., Gharib, M., Lane, B. & Mesquita, O.N. 1991 Fluctuations and transport in a stirred fluid with a mean gradient. *Phys. Rev. Lett.* **67**, 3507-3510.

Grossmann, S. & Lohse, D. 2000 Scaling in thermal convection: a unifying theory. *J. Fluid Mech.* **407**, 27-56.

Grossmann, S. & Lohse, D. 2001 Thermal convection for large Prandtl numbers. *Phys. Rev. Lett.* **86**, 3316-3319.

Grossmann, S. & Lohse, D. 2002 Prandtl and Rayleigh number dependence of the Reynolds number in turbulent thermal convection. *Phys. Rev. E* **66**, 016305

Holzer, M. & Pumir, A. 1993 Simple models of non-Gaussian statistics for a turbulently advected passive scalar. *Phys. Rev. E* **47**, 202-219.

Jayesh & Warhaft, Z. 1991 Probability distribution of a passive scalar in grid-generated turbulence. *Phys. Rev. Lett.* **67**, 3503-3506.

Kerr, R.M. & Herring, J.R. 2000 Prandtl number dependence of Nusselt number in direct numerical simulations. *J. Fluid Mech.* **419**, 325-344.

Kerstein, A.R. 1999 One-dimensional turbulence: model formulation and application to homogeneous turbulence, shear flows, and buoyant stratified flows *J. Fluid Mech.* **392**, 277-334.

Kimmel, S.J. & Domaradzki, J.A. 2000 Large eddy simulations of Rayleigh-Beńard convection using subgrid scale estimation model. *Phys. Fluids* **12**, 169-184.

Kraichnan, R. 1962 Turbulent thermal convection at arbitrary Prandtl number. *Phys. Fluids* **5**, 1374-1389.

Lam, S., Shang, X.-D., Zhou, S.-Q. & Xia, K.-Q. 2002 Prandtl number dependence of the viscous boundary layer and the Reynolds numbers in Rayleigh-Beńard convection *Phys. Rev. E* **65**, 066306.

Lohse, D. & Toschi, F. 2002 The ultimate state of thermal convection (preprint).

Niemela, J.J., Skrbek, L., Sreenivasan, K.R. & Donnelly, R.J. 2000 Turbulent convection at very high Rayleigh numbers. *Nature* **404**, 837-840.

Roche, P.-E., Castaing, B., Chabaud, B., Hebral, B. & Sommeria, J. 2001 Side wall effects in Rayleigh-Beńard experiments. *Eur. Phys. J. B.* **24**, 405-408.

Rossby, H.T. 1969 A study of Beńard convection with and without rotation. *J. Fluid Mech.* **36**, 309-335.

Siggia, E.D. 1994 High Rayleigh number convection. *Ann. Rev. Fluid Mech.* **26**, 137-168.

Takeshita, T., Segawa, T., Glazier, J.A. & Sano, M. 1996 Thermal turbulence in mercury. *Phys. Rev. Lett.* **76**, 1465-1468.

Tanaka, H. & Miyata, H. 1980 Turbulent natural convection in a horizontal water layer heated from below. *Int. J. Heat Mass Transf.* **23**, 1273-1281.

Verzicco, R. & Camussi, R. 1999 Prandtl number effects in convective turbulence. *J. Fluid Mech.* **383**, 55-73.

Verzicco, R. 2002 Sidewall finite-conductivity effects in confined turbulent thermal convection. *J. Fluid Mech.* **473**, 201-210. *J. Fluid Mech.* **383**, 55-73.

Wu, X.Z. & Libchaber, A. 1992 Scaling relations in thermal turbulence: the aspect-ratio dependence. *Phys. Rev. A* **45**, 842-845.

Wunsch, S. 1998 A simple passive scalar advection-diffusion model. *Phys. Rev. E* **58**, 5757-5764.

Wunsch, S. & Kerstein, A.R. 2001 A model for layer formation in stably stratified turbulence. *Phys. Fluids* **13**, 702-712.

Wunsch, S. 2003 Stochastic simulations of buoyancy-reversal experiments. *Phys. Fluids* **15**.

Xia, K.-Q., Lam, S. & Zhou, S.-Q. 2002 Heat-flux measurement in high-Prandtl-number turbulence Rayleigh-Beńard convection. *Phys. Rev. Lett.* **88**, 064501.